Synthesis, structural and magnetic characterization of Mn^{2+} doped ZnO nanopowders

R. Varadhaseshan [a], S. Ravi [b] S. Meenakshi Sundar [c],*
[a,c]PG and Research Department of Physics, Sri Paramakalyani College, Tirunelveli, India-627412
[b]PG and Research Department of Physics, National College, Trichy, India-620001
email: rvseshan@gmail.com

Abstract

ZnMnO nanopowders were prepared using microwave irradiation method. The structural and magnetic behaviors of the nanopowders were investigated. The x-ray diffraction patterns show wurtzite structure with no secondary phase in all samples. The increase in the lattice strain and crystal size due to the effect of Mn doping was confirmed by Williamson-Hall method. According to the magnetization measurements ferromagnetic behavior was found for $Zn_{0.9}Mn_{0.1}O$ combination. The observed ferromagnetism is due to the size effect and incorporation of Mn in Zn site in all probability.

Introduction

Zinc oxide is a group II-VI semiconductor compound and has a direct bandgap around 3.2-3.37eV in 300K with a high exciton binding energy of 60meV and is a wide bandgap semiconductor. This material has been used in a wide range of applications such as room temperature ultraviolet-lasers, transparent conducting electrodes, field-effect transistor, gas sensors, solar cells, optoelectronic devices, field emission devices and photoluminescence, Huang et al (2001), Owen et al (2007). ZnO is considered as a substitute to GaN and ITO, as transparent conducting oxide. It has high electrochemical stability and control over resistance (10^{-3} to 10^{-5} Ω). Therefore it is a potential candidate for optoelectronic applications in the short wavelength range (green, blue, UV), information storage and sensors, Jayalakshmi et al (2008), Lie et al (2006). Synthesis of these materials is often accomplished by sputtering, pulsed laser deposition (PLD), Molecular beam epitaxial (MBE), chemical vapor deposition (CVD), solid state reaction, ball milling and sol–gel techniques. In most of these methods, the nature of the produced material is amorphous and an additional high-temperature processing step is required in order to obtain crystallinity.

Researchers have carried out extensive studies of semiconductors, in which transition metal atoms are introduced into the lattice, thus inserting local magnetic moments into their lattice. In recent years, due to the prediction of possible ferromagnetic transition in metal-doped ZnO with a Curie temperature above room temperature research on ZnO:Mn has increased significantly Sharma et al (2003). The theory proposed by Dietl (2000) predicts room temperature ferromagnetism in Mn doped p-type ZnO. In addition to Dietl's prediction, ferromagnetism (FM) in magnetically doped ZnO has been theoretically investigated by *ab initio* calculations based on the local density approximation. Sharma et al. and V.K. Sarma et al. (2007) have carried out measurements on ZnO:Mn for the FM transition. One of the major challenges lies in preparing a ferromagnetic material having Curie temperature above room temperature.
A number of researcher have therefore investigated the ferromagnetic properties on Mn doped ZnO in the last few years. While some authors claimed to have evidence of the existence of room-temperature ferromagnetism in ZnMnO, others detected anti-ferromagnetic or paramagnetic behavior in this material Jayakumar et al (2006), Liu et al (2008). Most groups observe ferromagnetism at low temperatures. Some researchers have found ferromagnetism above room temperature for transition-metal-doped ZnO, Han et al (2002). This paper will focus on the formation and structural characterization of $Zn_{1-x}Mn_xO$ ($0.1 \leq x \leq 0.4$) using microwave synthesis. Recently, microwave irradiation has been widely applied to material science. Due to intense friction and the collision of molecules created by microwave irradiation, microwave irradiation not only provides the energy for heating but also greatly accelerates the nucleation. With

microwave irradiation on the reactant solution, temperature and concentration gradients can be avoided leading to uniform nucleation. Microwave-based synthesis method is one of the easiest, energy-saving, and quick methods for largescale production of nanomaterials.

It is significant to note that the microwave irradiation has several advantages over conventional methods including short reaction time, small particle size, narrow size distribution, and high purity, A.K. Singh et al (2008). This paper will focus on the formation and characterization of Manganese doped zinc oxide ($0.1 \leq x \leq 0.4$) using room temperature and microwave synthesize. The synthesis, structural, optical and magnetic properties of these samples will be discussed.

Experimental

The precursors utilized for the synthesis of ZnO:Mn, are Zinc acetate dihydrate, Manganese acetate tetra hydrate and ethylene glycol as solvent. All chemicals were purchased from Merck Company. All samples of ZnO:Mn, nanostructured particles were prepared by the microwave heating method. First at room temperature, zinc acetate and a dopant were dissolved in ethylene glycol solvent. Then the solution kept in a oven and microwave power was set to 650 watts and 2.5GHz operated in 30 second cycles for 20 minutes in total. The resulting powder was washed with distilled water and acetone and left to dry.

As prepared samples were characterized by X-ray diffraction (XRD) using a Rigaku diffractometer for the crystallographic measurements. The X-ray diffractometer was operated at 40 kV and 40 mA with Cu Kα radiation (λ=1.540598Å). The FTIR spectrum was recorded by Perkin Elmer make of Spectrum RXI model instrument in the range of 400cm^{-1} to 4000cm^{-1}. The morphology and composition of the synthesized samples were investigated by SEM & EDAX analysis (FEI Quanta FEG 200 High Resolution Scanning Electron Microscope). The TEM images were taken by Philips make Technai10 model. The magnetic properties of the powder sample were performed by EG & G PARC VSM 155 vibrating sample magnetometer.

Result and Discussion

The X-ray diffraction patterns (XRD) of the as prepared Mn doped ZnO powder sample were measured at room emperature shown in Fig.1 indicates highly c-axis oriented structure. To improve the crystallinity the samples were annealed at 400˚C and the XRD spectra were taken for all samples shown in Fig.2. The characteristic peaks with high intensities corresponding to the planes (100), (002), (101) and lower intensities of (102), (110), (103), (112) indicates the annealed product is of high purity hexagonal ZnO wurtzite structure. It is evident from the XRD spectra that there were no extra peaks due to Mn metal, other oxides or any zinc manganese phase, indicating that the as synthesized samples annealed at 400˚C are of single phase or that are not within the XRD resolution limit. But the shifting of peak in the XRD spectrum was noticed. Mn ions introduced as dopant at levels up to 40 at% shift the diffraction peaks to lower angles, indicating that the unit cell expands to accommodate the ions. This result is illustrated in Fig.3, which shows peak shifts of 0.19° in the (1 0 1) plane diffraction lines, 40 at% Mn-doped ZnO. Such a change is expected since Mn is known to substitutionally replace Zn in the lattice and has a larger ionic radius than Zn and changes lattice parameters. Using XRDA software, the lattice parameters *a* and *c* were calculated for the annealed samples. The parameters of Mn doped nanopowders were in good agreement with those reported in the JCPDS file for ZnO [PDF 79-206, *a* = 3.2499Å and *c* = 5.2065 Å]. This indicates that Mn doping might be the cause for some lattice disturbance in ZnO samples. The enhancement in the lattice constants is attributed to the strain in the crystal lattice due to the difference in ionic radius between Zn^{2+} and Mn^{2+} Mingxia Yuan et al (2009), Cuong Ton-That et al (2012). Higher concentration of Mn ions in ZnO would induce a larger strain in the nanopowders. Williamson-Hall method is used to find out the strain and size of the crystal Achamma George et al (2011). The increment of the unit cell volume correlates with the higher ionic radii of Mn^{2+} ions. The enhancement of unit-cell volume is almost linear with substitution of Mn. The morphology of the Mn doped ZnO samples were analyzed by SEM images which indicates the particles are spherical in shape with nanoscale size distribution shown in Fig. 4. The particle sizes were increasing with the increase of Mn

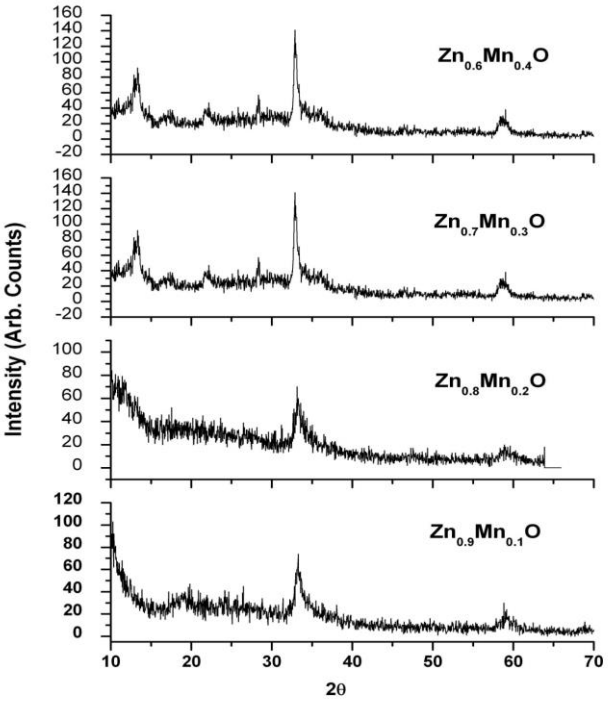

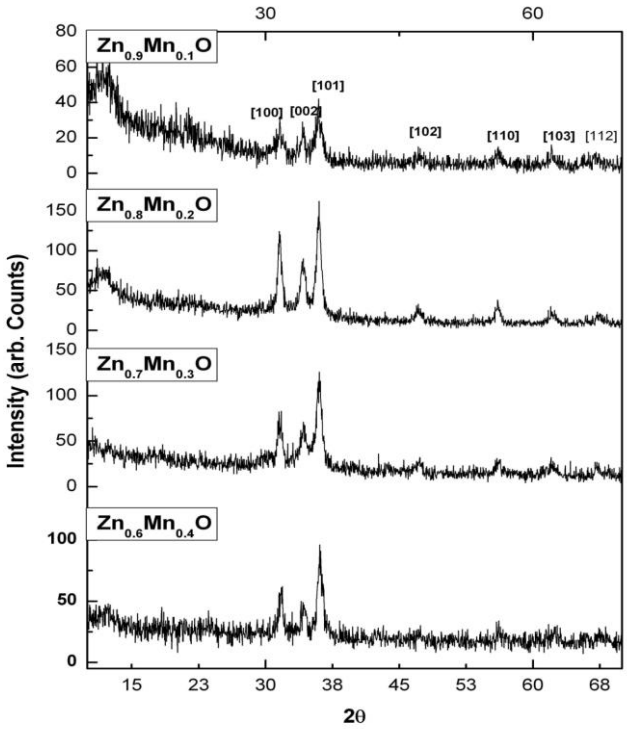

Figure 1 **Figure 2**

Figure 1: XRD pattern of as prepared Mn doped ZnO nanopowders

Figure 2: XRD pattern of Mn doped ZnO nanopowders annealed at 400˚C

concentration. The presence of elements like Zn, Mn, O were confirmed by Energy Dispersive Analysis of X-rays (EDAX) shown in Fig. 5. From the EDAX spectrum, increment of Mn content was noticed in the successive doping. TEM image of $Zn_{0.7}Mn_{0.3}O$ crystals size were confirmed as 15 nm shown in Fig. 6. It is known that the peak broadening occurs due to decrease in crystallite size and also the increase of lattice strain. The integral breadth of the peaks diffracted by crystals with volume defects can be written using Eq. (1).

$$\beta^T = \frac{\lambda}{L\cos\theta} \quad and \quad \beta^d = \eta\tan\theta \qquad (1)$$

With regard due to effect of size (or stacking faults, β^T), and widening induced by microstrain (β^d) respectively. But in our case, the contribution could be due to these two factors simultaneously. To calculate these two contributions, Williamson–Hall method is applied. It assumes that the size of the crystal and presence of crystallographic distortion lead

to lorentzian intensity distribution. If we denote by β_p the pure breadth and by β^T and β^d the breadths related to size and microstrains respectively, then we obtain Eq(2).

$$\beta_p = \beta^T + \beta^d \qquad (2)$$

Putting values from Eq. (1) in Eq. (2) and considering 'L' to be Lorentzian function,

We have

$$\beta p = \frac{\lambda}{L\cos\theta} + \eta\tan\theta \qquad (3)$$

Or

$$\frac{\beta p\cos\theta}{\lambda} = \frac{1}{L} + \frac{\eta\sin\theta}{\lambda} \qquad (4)$$

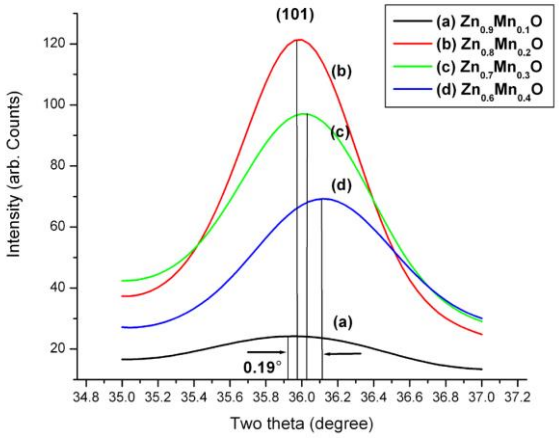

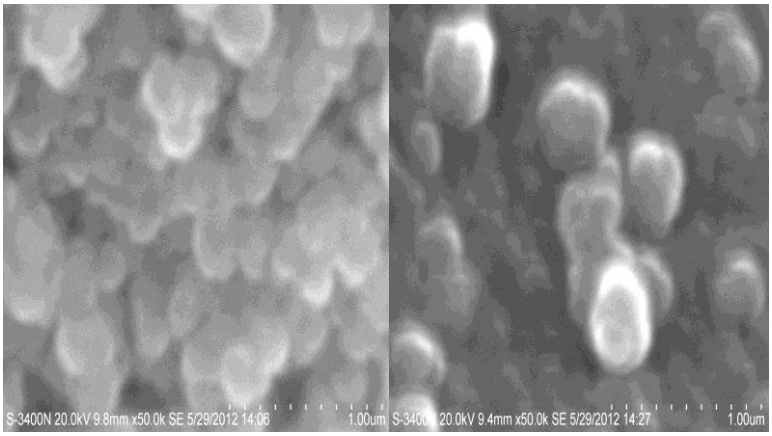

Figure 3 **Figure 4(a)** **Figure 4 (b)**

Figure 3: XRD peak shift of [101] plane in the $Zn_xMn_{1-x}O$ ($0.1 \leq x \leq 0.4$) nanopowders
Figure 4: SEM micrographs of (a) $Zn_{0.9}Mn_{0.1}O$ and (b) $Zn_{0.8}Mn_{0.2}O$ nanopowders

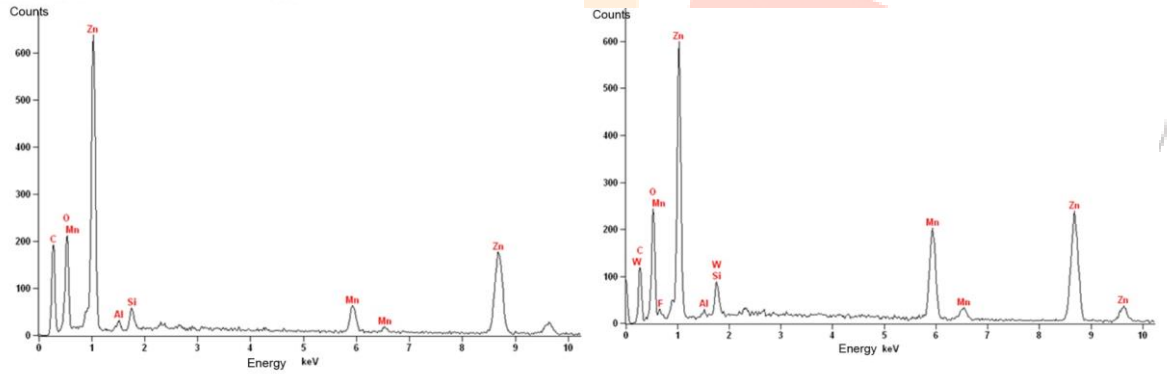

Fig. 5 (a) **Fig. 5 (b)**

Figure 5: EDAX spectrum of (a) $Zn_{0.9}Mn_{0.1}O$ and (b) $Zn_{0.8}Mn_{0.2}O$ nanopowders.

Hence, from the plot between $\frac{\beta p \cos\theta}{\lambda}$ and $\frac{\sin\theta}{\lambda}$ is a straight line with Y-intercept equal to the inverse of size and a slope equal to the value of the microstrain. It is clear that the experimental process induces a valuable strain in the specimen. Figure 7 shows the value of increase in microstrain (ε) with the increase in concentration of Mn up to 30 at %, further increase of Mn the strain reaches the saturation state. This analysis shows Mn doping has a major effect on the crystal size of the samples. If the strain increases, crystalline size also increases and it could be associated to increase of defects. The strain value reaches maximum saturated value at the doping concentration of Mn at 30 at%, further increase of Mn concentration no variation in the crystal size. It is thus concluded that Mn substitution definitely affects the lattice parameters of the crystalline structure of ZnO nanopowders in the present case. The texture coefficient (*TC*) represents the texture of the particular plane, deviation of which from unity implies the preferred growth. The quantitative information concerning the preferential crystal orientation can be obtained by the texture coefficient (TC). The different

texture coefficient TC (hkl) have been calculated from the x-ray data using the well-known formula and it is defined as, Pankove (1971), Barret (1980) Ramadan et al (2009)

$$TC(hkl) = \frac{I(hkl)/I_0(hkl)}{1/n \sum I(hkl)/I_0(hkl)} \qquad (5)$$

where *I(hkl)* is the measured relative intensity of a plane *(hkl)*, $I_o(hkl)$ is the standard intensity of the plane *(hkl)* tak en from the JCPDS data, *n* is the number of diffraction peaks. If *TC(hkl)* ≈1 for all the *(hkl)* planes considered, then the films are with a randomly oriented crystallite similar to the JCPDS reference, while values higher than 1 indicate the abundance of grains in a given *(hkl)* direction. Values 0<*TC(hkl)*<1 indicate the lack of grains oriented in that direction. As *TC(hkl)* increases, the preferential growth of the crystallites in the direction perpendicular to the hkl plane is the greater. Since three diffraction peaks were used ((100), (002), (101)), the maximum value *TC(hkl)* possible is 3. The values of texture coefficient calculated for the main diffraction peaks from Fig. 3 are summarized. One can be seen that respective *TC* (hkl) values are deviated from unity value (corresponding to non-textured sample) especially that for (002) peak. This fact confirms the preferred c-axis orientation of crystallites in respective sample. Similar (002) texture was reported for Mn doped ZnO thin films, Liu et al (2005). The synthesized sample annealed at 400ºC have the preferred orientation, with highest texture coefficient, along (101) plane. If the concentration of Mn increases the texture coefficients (TC) are approximately decreases for the planes (100) and (002) and in the mean time TC increases in the (101) plane orientation which is shown in Fig. 8. Thus the preferred orientation changes from (100) to (101) reflection plane for the synthesized nanopowders annealed at 400ºC.

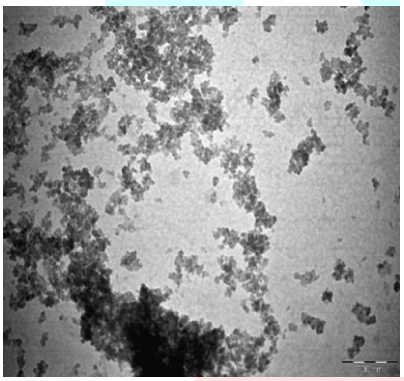

Fig. 6

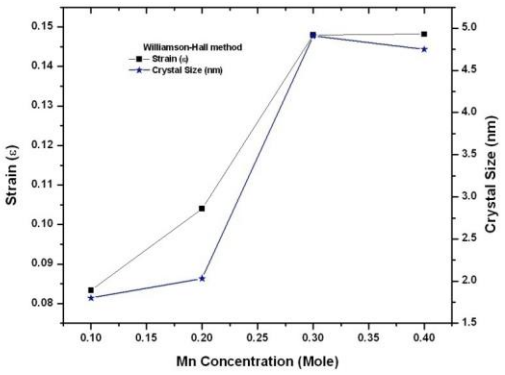

Fig. 7

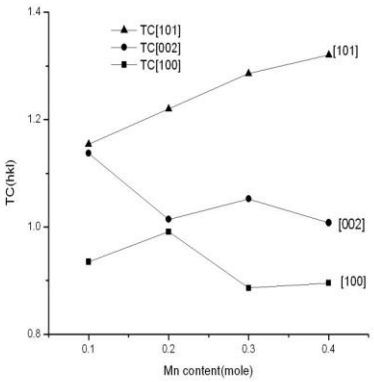

Fig. 8

Figure 6: TEM image showing the well dispersed particles of $Zn_{0.7}Mn_{0.3}O$ nanopowders
Figure 7: Plot of Mn doping concentration Vs Crystal size and strain by Williamson-Hall method.
Figure 8: Texture coefficients for various lattice plane values with the preferred orientation of [101] of ZnMnO nanopowders

Fig. 9 shows the FT-IR spectrum of Mn doped ZnO nanopowders annealed at 400ºC with different mole ratios (10 to 40 moles %) respectively. For FT-IR analysis the KBr pellets are prepared from the different mole % of Mn doped ZnO nanopowders. The broad peak in higher energy in the region at 3600 – 3400 cm^{-1} is due to OH stretching or it may be due to the M-OH-M, V.D. Mote et al (2011). The principle absorption peaks are observed between 1650 – 1400 cm^{-1}, corresponding to the stretching frequency of the carboxyl group (C=O), Senthilkumaar et al (2008). The peak in the range 1400-1757 cm^{-1} is due to OH bending of adsorbed moisture in the sample and the peaks around 2900 cm^{-1} is due to C–H (acetate) stretching. The deformation bands of C=O can also be observed around 1000 cm^{-1}, Alaria et al (2005). Similarly the bands at 780-980 cm^{-1} might be due to the peroxide formation (M-O-O-M) sample and all the other peaks are attributed to the characteristic of the material. In all mole rations of Mn doped ZnO around 1400 cm^{-1} peak occurs

due to CH_2 bending mode. In all samples the main absorption band is due to Zn-O and (Zn,Mn)- O stretching in the range of 700 cm^{-1} - 400 cm^{-1}. FT-IR spectra of the present investigation are similar to that of Mn doped ZnO samples are in good agreement with the reported values, Dole et al (2011).

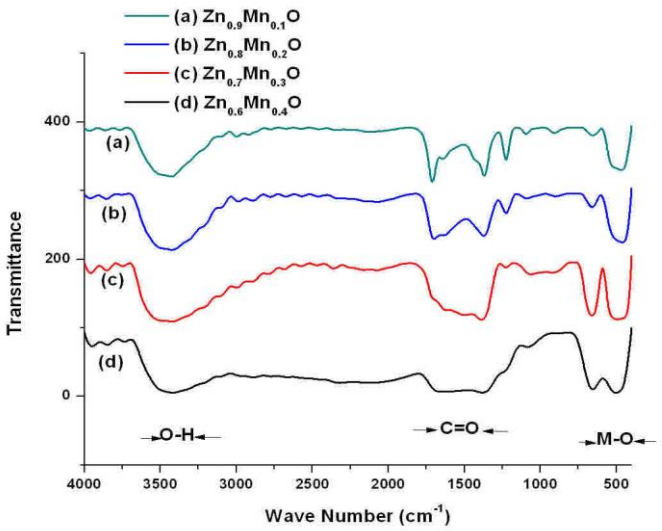

Fig. 9

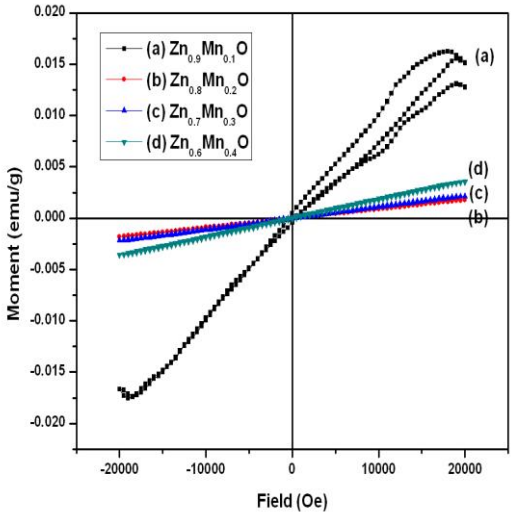

Fig. 10

Figure 9: FTIR spectrum of Mn doped ZnO nanopowders system
Figure 10: VSM images of $Zn_{1-x}Mn_xO$ ($0.1 \le x \le 0.4$) shows the ferromagnetism at (x=0.1), for higher Mn concentration (x=0.2 to 0.4) the system exhibits paramagnetism.

Magnetic behavior of Mn doped ZnO

Pure ZnO is diamagnetic and its matrix can be made ferromagnetic by replacing some atoms of Zn with impurities. The *M–H* curve measured for $Zn_xMn_{1-x}O$ samples at room temperature was obtained up to magnetic field range ±20 kOe shown in Fig. 10 which indicates a ferromagnetic hysteresis loop at x=0.1 at mole %. The coercivity (Hc) value and the remanent magnetization are 426 Oe and 4.43×10^{-4} emu/g respectively. Room Temperature ferromagnetism (RTFM) was also found in Mn-doped ZnO nanoparticles by J.H Lie al (2006). According to RKKY theory, the ferromagnetic behavior arises as a result of the exchange interaction between local spin-polarized electrons (such as the electrons of Mn^{2+}) and conductive electrons, V.K. Sharma et al (2007) and Priour Jr. et al (2004). The saturation magnetization obtained for Mn concentration 0.1 at mole % is 16×10^{-4} emu/g. P.Sharma *et al*. (2003) reported that the lower values of saturation magnetization might be due to the smaller sizes of crystallites in the samples, *Murtaza Saleem et al*. (2010), also confirmed this lowest saturation magnetization value in his work. But for higher dopant ratio x>0.1M the samples exhibit paramagnetic state shown in Fig. 8, these curves display a Curie behavior and the data could be fitted to a straight line confirming the existence of pure paramagnetism. This might be due to the dominant antiferromagnetic interaction between the Mn^{2+} ions over the expected ferromagnetism. However, the origin of the ferromagnetism is still in debate, because the substitution of equal valence ions is electrically equivalent, which is not consistent with Dietl's hole induced ferromagnetism theory. Magnetic behavior of the same material might be rather different when it was investigated in powder, bulk or thin film forms. This effect arises due to the dependence of magnetic behavior on the structural arrangement. When the material is investigated in powder form, the surface of every particle behaves independently and is induced strongly by the other neighboring particles. Consequently, the disturbance in magnetic interactions can be observed due to this surface and inter-particle boundary connections. The parent ZnO material is of diamagnetic behavior and the substitution of Mn in the Zn sites of ZnO forms the ferromagnetism in our

$Zn_{1-x}Mn_xO$ nanopowders with x=0.1. The observed existence of ferromagnetism could not be from Mn-related secondary phases MnO_2, Mn_2O_3, Mn_3O_4, and/or MnO, since XRD analysis did not show their presence. The magnetization curve proves that ferromagnetic ordering arises from ZnMnO in all probability.

Conclusion

Based on the structural analysis, it was found that the doping metals like Mn^{2+} have a significant role on lattice strain and parameters. RTFM was observed in $Zn_{0.9}Mn_{0.1}O$ nanopowder system due to the size effect and exchange interaction between local spin polarized electrons of Mn^{2+} and conduction electrons. The paramagnetic behavior was observed for higher doping ratio of Mn (x=0.2 to 0.4) due to the decrease of distance between Mn^{2+} ions which leads antiferromagnetic interaction which suppresses the resultant ferromagnetic behavior.

Acknowledgement

This work was financially supported by the University Grant Commission (UGC) India,from the Major Research Project scheme (F.No.39-451/2010). The authors thanks to UGC for providing financial support to do this work.

Reference

Achamma George, Suchinder K. Sharma, Santa Chawla, Malik M.M., Qureshi M.S., J. Alloys Compd.

Detailed of X-ray diffraction and photoluminescence studies of Ce doped ZnO nanocrystals 509 (2011) 5942–5946.

Alaria J., Turek P., Bernard M., Bouloudenine M., Berbadj A., Brihi N., No ferromagnetism in Mn doped ZnO semiconductors, Chem. Phys. Lett. 415 (2005) 337.

Barret C. S., Massalski T.B., Structure of Metals, Pergamon Press, Oxford, 1980, pg.204.

Cuong Ton-That, Matthew Foley, Matthew R.Phillips, Takuya Tsuzuki, Zoe Smith, Correlation between the structural and optical properties of Mn-doped ZnO nanoparticles, J. Alloys Compd. 522 (2012) 114.

Dietl T., Ohno H., Matsukura F., Cibert J., Ferrand D., Zener model description of ferromagnetism in Zinc-Blende magnetic semiconductors, Science 287 **(**2000**)** 1019.

Dole B.N., Mote V.D., Huse V.R., Purushotham Y., Lande M.K., Jadhav K.M., and Shah S.S., Structural studies of Mn doped ZnO nanoparticles, Cur. Appl. Phys.11 (2011) 762.

Han S.J., Song J.W., Yang C.H., Park J.H., Jeong Y.H., Rhie K.W., A key to room-temperature ferromagnetism in Fe-doped ZnO:Cu, Appl. Phys. Lett. 81 (2002) 4212.

Huang M.H, Mao S., Feick H., Yan H., Wu Y., Kind H., Weber E., Russo R., Yang P., (2001) Room-temperature ultraviolet nanowire nanolasers, Science, 292, 1897.

Jayakumar O.D., Salunke H.G., Kadam R.M., Mohapatra M., Yaswant G., Kulshreshta S.K., (2006) Magnetism in Mn-doped ZnO nanoparticles prepared by a co-precipitation method, Nanotechnology 17 , 1278.

Jayalakshmi M., Palaniappa M., Balasubramanian B., (2008) Single step solution combustion synthesis of ZnO/carbon composite and its electrochemical characterization for supercapacitor application, Int. J. Electrochem. Sci. 3, 96.

Li J.H., Shen D.Z., Zhang J.Y., Zhao D.X., Li B.S., Lu Y.M., Liu Y.C., Fan X.W., (2006) Magnetism origin of Mn-doped ZnO nanoclusters, J. Magn. Magn. Mater, 302, 118.

Lie L., Zhang Y., Mao S.S., Lin L., (2006) Fabrication and characterization of ZnO nanowires based UV photodiodes, Sens. Actuat.: A 127 201.

Liu C., Yun F., Xiao B., Cho S.J., Moon Y. T., Morkoc H., Abouzaid M., Ruterana R., Yu K. M., Walukiewicz W., (2005) Structural analysis of ferromagnetic Mn-doped ZnO thin films deposited by radio frequency magnetron sputtering, J. Appl. Phys., 97, 126107.

Liu Z.W., Yang S.G., Raju V. Ramanujan , Ong C.K., (2008) Confirmation of room temperature ferromagnetism for Mn-doped ZnO micro-tetrapod powders, Materials Letters 62, 1255.

Mingxia Yuan, Wuyou Fu, Haibin Yang, Qingjiang Yu, Shikai Liu, Qiang Zhao, Yongming Sui, Dong Ma, Peng Sun, Yanyan Zhang, Baomin Luo, (2009) Structural and magnetic properties of Mn-doped ZnO nanorod arrays grown via a simple hydrothermal reaction, Materials Letters 63 , 1574.

Mote V.D., Purushotham Y., Dole B. N., (2011) Structural and morphological studies on Mn substituted ZnO nanometer-sized crystals, Cryst. Res. Technol. 46 705.

Murtaza Saleem, Saadat A. Siddiqi, Shahid Atiq, M. Sabieh Anwar, Saira Riaza, (2010) Room temperature magnetic behavior of sol-gel synthesized Mn doped ZnO, Chinese Journal of Chemical Physics volume 23, 4, 469.

Owen J., Son M.S., Yoo K.H., Ahn B.D., Lee S.Y., (2007) Organic photovoltaic devices with Ga-doped ZnO electrode, Appl. Phys. Lett. 90, 033512.

Pankove J.I., (1971)Optical Processes in Semiconductors, Prentice-Hall Inc., Englewoord Cliffs, New Jersey, USA ,.

Priour Jr. D.J., Hwang E.H., Sarma S.D., (2004) Disordered RKKY lattice mean field theory for ferromagnetism in diluted magnetic semiconductors, Phys.Rev. Lett. 92, 117201

Ramadan A.A., Abd El-Mongy A.A., El-Shabiny A.M., Mater A.T., Mostafa S. H., El-Sheheedy E. A., Hashem H. M., (2009) Addressing difficulties in using XRD intensity for structural study of thin films, Cryst. Res. Technol., 44, 111.

Senthilkumaar S., Rajendran K., Banerjee S., Chini T.K., Sengodan V., (2008) Influence of Mn doping on the microstructure and optical property of ZnO, Materials Science in Semiconductor Processing 11 , 6.

Sharma P., Gupta A., Rao K.V., Owens F.J., Sharma R., Ahuja R., Osorio Guillen J.M., Johansson B., Gehring G.A., (2003)Ferromagnetism above room temperature in bulk and transparent thin films of Mn-doped ZnO, Nature 2 , 673.

Sharma V.K., Xalxo R., and Varma G.D., (2007) Structural and magnetic studies of Mn-doped ZnO Cryst. Res. Technol. 42 , 34.

Singh A.K., Vijay, S. Raykar, (2008) Microwave synthesis of silver nanofluids with polyvinylpyrrolidone (PVP) and their transport properties, Colloid Polym. Sci. 286,1667.